Circumstellar silicon chemistry and the SiO maser

Clegg, R.E.S.; Ijzendoorn, L.J. van; Allamandola, L.J.

Mon. Not. R. astr. Soc. (1983) **203**, 125–146

Circumstellar silicon chemistry and the SiO maser

R. E. S. Clegg,* L. J. van IJzendoorn and
L. J. Allamandola *Laboratory Astrophysics, Huygens Laboratorium, University of Leiden, PO Box 9504, 2300 RA Leiden, The Netherlands*

Received 1982 June 7; in original form 1982 February 4

Summary. We have investigated the effects of stellar chromospheric UV radiation on the composition of gaseous layers around O-rich red-giant stars losing mass, with particular attention to the almost static layers recently identified from infrared spectra. The UV radiation can strongly inhibit molecular association. Si-chemistry is studied in the steady-state approximation, and some simple results concerning time-scales, shell optical depths and photoelectric heating rates are deduced. Around α Orionis we predict that CO should be fully associated but that hydrogen should be in atomic form. We show that a chemical pump for SiO masers would operate too slowly to explain the observed photon emission rate, and propose some observational diagnostics of circumstellar molecular processes.

1 Introduction

The shells of gas and dust around late-type stars have been studied intensively in the last few years by spectroscopic techniques at all accessible parts of the electromagnetic spectrum; a recent review has been given by Zuckerman (1980). However, few studies of the chemical processes which can take place in the circumstellar (C/S) flowing gas have been made. Scalo & Slavsky (1980) have discussed the relevant time-scales (expansion, chemical reaction and photodissociation/ionization) around O-rich red giants. Goldreich & Scoville (1976) examined the C/S chemistry of H_2O and OH while Clegg & Wootten (1980) studied Cl chemistry and the H–H_2 system. In this paper the reactions taking place in the gas around M-type supergiants are modelled and α Orionis (M2 Iab) is used as a prototype, since it is the nearest such star and well observed.

We postulate that these reactions take place in a region between $2–12R_*$ or even $2–50R_*$ which is mostly gaseous, has a low expansion velocity, $v_e \leqslant 3\,\mathrm{km\,s^{-1}}$, and so does not contribute to the violet-shifted C/S optical absorption lines. Although typical expansion

* Present address: Department of Physics and Astronomy, University College London, Gower Street, London WC1.

velocities lie in the range 10–20 km s^{-1} (see Zuckerman 1980) these velocities are not attained until a considerable distance from the star is reached. Evidence for the existence of such a low velocity, primarily gaseous shell is provided by the following. Bernat (1977) finds, from an analysis of the Ca II infrared line profiles, that the inner radius for the α Ori shell is $50R_*$ while Sutton *et al.* (1977) and McCarthy, Low & Howell (1977) deduce from IR interferometry at 11 μm that most of the C/S dust emission from α Ori originates from outside 12 or $25R_*$ respectively. Furthermore, from observations of the Mg II resonance lines, Bernat & Lambert (1976) suggested that a cool turbulent region exists between the α Ori chromosphere (which may extend to $2R_*$) and the accelerated C/S flow. Such a region must be optically thin in the visible and near UV but not necessarily in the far UV ($\lambda \leqslant 1500$ Å) because of absorption due to atomic and molecular transitions. Small grains may already exist in this region but, owing to inherently low emissivity at 11 μm, be undetectable. If present, these cores could provide the condensation nuclei essential for subsequent large grain growth and, by collision with the non-condensables, accelerate the gas continuously (see Draine 1980).

While models of the α Ori dust shell by Rowan-Robinson & Harris (1982) do contain an inner spherical cavity of radius $12–50R_*$ it should be realized that other interpretations of some of the observational data exist; for example, using similar data Sanner (1976) deduced inner shell radii much smaller than those of Bernat (1977) and such Mg II line profiles have also been interpreted in terms of expansion in the chromosphere itself (Stencel & Mullan 1980).

While the situation around long-period variable stars (LPV) is envisaged to be slightly different, the model described here and conclusions drawn are applicable to these stars as well. Instead of a classical 'chromosphere' outside the stellar photosphere, a shock wave probably produces a heated region which moves through the stellar atmosphere during each pulsation period (Willson & Hill 1979; Hinkle 1978). Emission lines and ultraviolet radiation will originate in the shocked region. Most of the UV radiation must be absorbed by the outer atmosphere and any C/S dust. A layer of gas with $T = 1000$ K and low velocity amplitude was identified by Hinkle around R Leo, an O-rich LPV which shows SiO maser emission. Our calculations apply to this region in the case of the LPV stars.

We present here a study of Si chemistry in the postulated shell which is likely to be cool ($T \leqslant 1000$ K) yet bathed in the chromospheric ultraviolet radiation (hereafter referred to as the cool region). The study of C/S silicon chemistry is of particular interest for a number of reasons.

First, because the 9.7 μm silicate feature is seen from α Orionis and from O-rich cool stars losing mass, we wish to know the likely composition of the C/S gas from which silicate grains condense or accrete. Secondly, we wish to determine whether the non-detection of SiO ($J = 2–1$) thermal emission from α Ori (Lambert & Vanden Bout 1978) may be due to photodissociation by stellar UV radiation or because all the Si atoms are bound up in the grains, as has been previously assumed. And thirdly, since VLBI results (Moran *et al.* 1979) have shown that SiO maser emission from late-type stars must be located close to the star it is attractive to consider the possibility that the masing medium is located in this 'cool region'. Maser emission is observed from excited vibrational levels of SiO. Because chemical reactions can populate such excited levels regardless of the local gas kinetic temperature and can produce daughter molecules with an inverted rotational population (e.g., Gericke, Ortgies & Comes 1980) we have investigated whether a chemical pump for the SiO maser could operate. We show that chemical pumping rates are too slow. We also investigate vibrational excitation via UV pumped fluorescence and find that this excitation channel also falls short of maintaining the necessary vibrational population.

The purpose of this paper is to present calculations made in the steady-state approximation, of the composition of gas located near the chromosphere of an early M-type supergiant. Results relevant for conditions around cooler stars and perhaps Mira variables are also presented. Although Scalo & Slavsky (1980) concluded that strict chemical equilibrium is never attained in a cool expanding circumstellar shell, we show in Section 3(a) below that the steady-state approximation is valid for most species, the H–H_2 system being a possible exception. The results of these calculations are applied to the C/S gas around a star such as α Orionis (Sections 3–7) and then to the problem of chemical pumping of the SiO maser around cooler stars (Section 8).

2 Calculations

2.1 CHOICE OF PHYSICAL PARAMETERS

In this section we discuss the following parameters: expansion velocity (v_e), gas density (n), kinetic temperature (T), UV radiation field (F_λ) and chemical composition. For a spherical shell expanding at constant velocity we may write, assuming no time dependence;

$$\rho v r^2 = \text{constant} \tag{1}$$

in which ρ is the gas density, v is the outflow velocity and r is the radius to the star.

In this model we are interested in an inner region in which it is assumed that $v = v_e$ = constant. The α Ori terminal flow velocity is 15 km s^{-1} (Knapp, Phillips & Huggins 1980), although optical C/S resonance lines give 11 km s^{-1} (Bernat 1977). Clearly the C/S gas must accelerate to the observed terminal velocity but the assumption of a constant v is justified for the level of accuracy that this study can achieve. We assume no contribution to the violet-shifted C/S components (so $v_e \leqslant 3$ km s^{-1}) and take a value of $v_e = 1$ km s^{-1}.

Equation (1) then may be rewritten in terms of the total particle density n:

$$n = 4 \times 10^8 \left(\frac{\dot{M}}{10^{-6} M_\odot \text{ yr}^{-1}}\right)\left(\frac{R}{10^{14} \text{ cm}}\right)^{-2}\left(\frac{v_e}{10 \text{ km s}^{-1}}\right)^{-1} \text{cm}^{-3}. \tag{2}$$

For our standard star, α Ori, we adopt $\dot{M} = 2 \times 10^{-6} M_\odot$ yr^{-1} (Knapp *et al.* 1980) and $R_* = 7.0 \times 10^{13}$ cm (Welter & Worden 1980) which, together with the outflow velocity $v_e = 1$ km s^{-1}, results in densities of 3×10^9 cm^{-3} at $R = 2R_*$ and 5×10^6 cm^{-3} at $50R_*$.

In general equation (2) also applies around a LPV, but the cool layer around R Leo described by Hinkle (1978) was not observed to have a net expansion velocity and thus its density may be larger than 10^{10} cm^{-3}. Hinkle estimated that $n_{H_2} \sim 10^{12}$ cm^{-3}.

The temperature of the gas around the supergiants is uncertain. In a model chromosphere for α Ori (Basri, Linsky & Eriksson 1981), the temperature minimum is estimated to be 2700 K and the maximum 7000 K. Outside the chromosphere the gas cools and grains form. Further away from the star, cooler regions of gas are detectable through CO vibration–rotation line profiles. For example, in the α Ori shell, CO lines show expansion velocity components of 11 and 18 km s^{-1}, which have temperatures of 200 and 70 K respectively (Bernat *et al.* 1979). The radius of the 18 km s^{-1} shell inner edge is $\sim$ 10 arcsec or $\sim 400R_*$ (Knapp *et al.* 1980). The M supergiants and Mira variables apparently do not have hot coronae. Around the LPVs we have assumed that the 1100 K shell seen by Hinkle is typical; and that the expanding gas further out has an initial temperature close to this.

Our procedure has been to select an initial temperature, $T_0 = 1100$ K, for both the M supergiant shell and the Mira variable shell. We let the local gas kinetic temperature vary as $T(R) \propto R^{-\alpha}$. For the adiabatic expansion of monatomic and diatomic gases, $\alpha = 4/3$ and

4/5 respectively. Detailed modelling of O-rich shells by Goldreich & Scoville (1976) suggests that T is constant between 1×10^{14} and 4×10^{14} cm and that effective cooling with $\alpha = 0.8$ occurs further out. One of the major heating sources they considered, grain–gas collisions, is not applicable in our case; however, as shown below, photoelectric heating should be included when there is chromospheric UV radiation. This heating term is smaller than that due to the grain–gas collisions and we therefore adopt the relations: T = constant = 1100 K ($R = 2$–$5\,R_*$) and $T \propto R^{-1}$ ($R > 5\,R_*$).

The ultraviolet radiation field used is based on the measured UV flux from α Ori. This flux is taken as the standard level, and the effects of a lower UV flux level from, say, a later-type M supergiant or LPV are examined.

α Ori has been chosen because it has been observed by the *TD-1*, *ANS* and *IUE* satellites, is close to the Sun and has no hot companion. The adopted flux curve is shown in Fig. 1. Symbols show the intermediate band ($\Delta\lambda \sim 150$ Å) fluxes from the *ANS* satellite (Van Duinen *et al.* 1975) and the *TD-1* satellite (Thompson *et al.* 1978). The *IUE* data were taken from Basri *et al.* (1981) and B. Haisch (private communication). The flux curve shown represents a smoothed version of the actual UV spectrum, which consists of many emission lines superimposed on a weak continuum which is observable down to about 1250 Å. For example, a Si II doublet near 1816 Å is particularly strong and has a peak intensity of 7.8×10^{13} erg cm^{-2} s^{-1}. Fig. 1 also shows some relevant blackbody fluxes; note that the equivalent temperature rises with decreasing wavelength. This has two probable causes: the flux contains many emission lines, and the continuous opacity increases with decreasing wavelength in the chromosphere, so that at shorter wavelengths unit optical depth is reached at higher and hotter layers. The adopted flux curve is described by the formula $F_\lambda \propto \exp(-\alpha/\lambda)$, where $\alpha = 1.4 \times 10^{-4}$ cm and the value at 2000 Å is taken to be 4.0×10^{-13} erg cm^{-2} s^{-1} Å^{-1}.

We have assumed that the dust optical depth in the α Ori shell is small for wavelengths longer than 1200 Å. The relevant depth is that for pure absorption, because light scattered by the C/S dust is observed if the detector entrance aperture is large compared to the shell (this is the case for the *IUE* observations). McMillan & Tapia (1978) found that, in the blue,

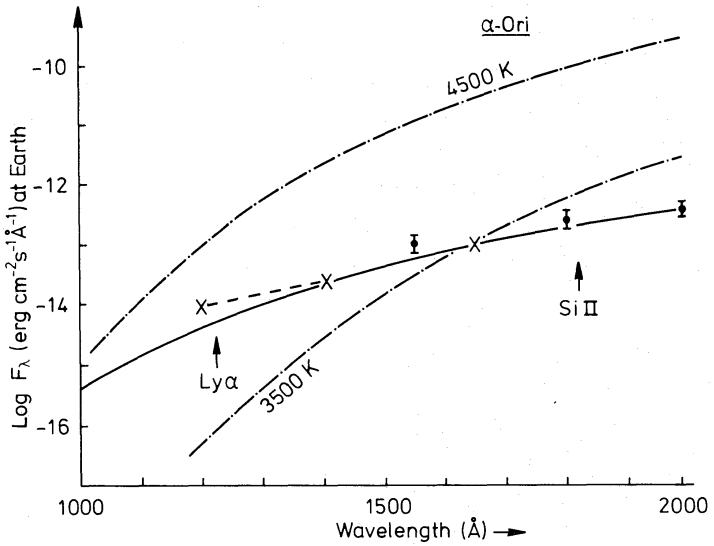

Figure 1. Ultraviolet flux of α Orionis. Solid dots – data from *TD-1* and *ANS*; crosses and dashed line – smoothed curve from *IUE* spectra. The solid curve gives our adopted fit, while the dash–dot lines show blackbody curves for the labelled temperatures, for radius $R = 2\,R_*$. The 'flat continuum' levels adopted by Stickland & Sanner (1982) are 1.7×10^{-14} (units as for ordinate) at 1250 Å and 1.6×10^{-13} at 1850 Å.

$\tau(\text{scatt}) \leqslant 0.15$, from which we have $\tau(\text{scatt}) \leqslant 0.35$ at 1200 Å for a grain albedo independent of wavelength. Lee (1970) gives $A_V = 0.5$ for this star, which translates into an extinction optical depth at 1200 Å of 1.5 if the average interstellar absorption properties apply here. The conclusion is that the *absorption* optical depth for $\lambda \geqslant 1200$ Å is probably less than 1. Stickland & Sanner (1981) have shown that there is little scattered light in the *IUE* spectra and that in addition to the emission lines, a flat continuum exists in the far UV spectrum of α Ori. Comparison with their adopted continuum level at 1250 Å shows that our F_λ value is 50 per cent lower because we initially allowed for some contribution from scattered light to the *IUE* spectra. Therefore we note that we may have *underestimated* the far UV α Ori flux and that a flat continuum is likely to be present at wavelengths below 1200 Å, where no spectra exist. Little is known about UV fluxes from stars cooler than α Ori. Examination of the *ANS*, *TD-1* and *IUE* records suggest that no such star without a hot companion has been detected at wavelengths below 2500 Å. Around these stars the chromospheres may be weaker and the dust UV optical depth larger than for α Ori.

The chemical composition of the C/S gas was taken to be the solar mixture of H, O, Si, S, Fe, Mg, Na and Ca. Ionization and recombination reaction involving the latter five elements were included to compute the electron density.

2.2 REACTION NETWORK

We have calculated the steady–state concentration of the atoms, ions and 11 molecules composed of Si, O and H. The chemical reactions and adopted rates are listed in Table 1. The photodissociation and photoionization reaction rates are shown in Table 2. These photo-rates are calculated for the UV flux density at $2R_*$ (1.4×10^{14} cm) from α Ori. Note that this flux is independent of the assumed distance from the Earth to α Ori, because the stellar angular diameter is known. The part of the reaction network which encompasses all the Si-chemistry is shown schematically in Fig. 2: the three sections I, II and III indicated in Fig. 2 refer to corresponding groups of reactions in Table 1. Only the forward (i.e. exothermic) reactions are shown; reverse reactions were included in the calculations (except for dissociative recombinations) and their rates were obtained by adding the net change in the Gibbs free energy, ΔG, to the activation energies. The reaction rates are given in the form: $k = AT^\alpha \exp(-E_a/T)\,\text{cm}^{-3}\,\text{s}^{-1}$ where A is the pre-exponential factor, T the gas kinetic temperature in K, α the temperature exponent and E_a the activation energy in K. α is non-zero only for electron recombinations with atomic ions. The assumption is made that the vibrational and rotational temperatures equal the local gas kinetic temperature. This is only acceptable in view of the uncertainties in many of the rates. In principle T_{vib} and T_{rot} do not equal the gas kinetic temperature because radiative transitions compete with collisions. It must be emphasized that, while nearly all of the rates involving O and H containing molecules have been measured, only three reaction rate measurements are available for the Si-bearing molecules.

The majority of the values used are estimates based on the rates used by Prasad & Huntress (1980) and Millar (1980). Rates for reactions involving Si and O were estimated by analogy with equivalent measured reactions involving sulphur atoms. It was assumed that the neutral–neutral reactions have activation energy barriers. We adopt 4.0 kcal/mol (2000 K) as typical for the radical–molecule reactions and 6.0 kcal/mol (3000 K) for the reactions between two stable molecules. The pre-exponential factor A was adjusted to produce a net rate at 1000 K equal to the rate estimated by Prasad & Huntress (1980). Because the activation energies are uncertain, separate calculations were also made in which E_a was taken to be zero for the radical–molecule reactions. Si atoms and OH radicals were

Table 1. Chemical reactions and rates.

Group	Reaction	$E_a[k]$	A	Ref.	Label
I A	$SiO + O \rightarrow SiO_2$	2500	1×10^{-17}	1	
	$SiO_2 + O \rightarrow O_2 + SiO$	2500	5×10^{-12}	1	
	$SiO + H_2O \rightarrow SiO_2 + H_2$	3000	5×10^{-13}	1	
	$SiO + OH \rightarrow SiO_2 + H$	2000	2×10^{-11}	1	
I B	$SiH + O \rightarrow SiO + H$	2000	1×10^{-11}	3, 4	
I C	$Si + O \rightarrow SiO$	0	1×10^{-17}	1	
	$Si + OH \rightarrow SiO + H$	2000	2×10^{-10}	2, 4	
	$Si + O_2 \rightarrow SiO + O$	2000	1×10^{-10}	1	
	$Si + H_2O \rightarrow SiO + H_2$	2000	1×10^{-10}	1	
I E	$SiOH^+ + e^- \rightarrow SiO + H$	0	4×10^{-7}	4	a
II A	$SiH + O_2 \rightarrow SiO_2 + H$	2000	1×10^{-11}	1	
II B	$SiH + O \rightarrow Si + OH$	2000	3×10^{-12}	1	
	$SiH + H \rightarrow Si + H_2$	2000	1×10^{-11}	1	
	$Si + H \rightarrow SiH$	0	1×10^{-16}	1	
II C	$SiO^+ + e^- \rightarrow Si + O$	0	1×10^{-7}	2	
II D	$SiO^+ + H_2 \rightarrow SiOH^+ + H$	0	3.2×10^{-10}	5	
III A	$SiH_2^+ + e^- \rightarrow SiH + H$	0	5×10^{-7}	4	
III C	$SiH^+ + e^- \rightarrow Si + H$	0	1×10^{-7}	2	
III D	$Si^+ + OH \rightarrow SiO^+ + H$	0	1×10^{-9}	4	b
	$SiO^+ + O \rightarrow Si^+ + O_2$	0	2×10^{-10}	5	c
	$Si^+ + O \rightarrow SiO^+$	0	1×10^{-17}	1	
III E	$Si^+ + H_2O \rightarrow SiOH^+ + H$	0	2.3×10^{-10}	5	d
III F	$SiOH^+ + e^- \rightarrow Si + OH$	0	2×10^{-7}	1	
III G	$Si^+ + H \rightarrow SiH^+$	0	1×10^{-17}	4	
	$SiH^+ + H \rightarrow Si^+ + H_2$	0	1×10^{-9}	4	
III H	$Si^+ + H_2 \rightarrow SiH_2^+$	0	1×10^{-15}	2	

Electron recombinations

Reaction	A	α	Ref
$Ca^+ + e^- \rightarrow Ca$	1.4×10^{-10}	−0.69	8
$S^+ + e^- \rightarrow S$	1.4×10^{-10}	−0.63	6
$Na^+ + e^- \rightarrow Na$	1.4×10^{-10}	−0.69	8
$Si^+ + e^- \rightarrow Si$	1.5×10^{-10}	−0.64	6
$Fe^+ + e^- \rightarrow Fe$	1.5×10^{-10}	−0.65	6
$Mg^+ + e^- \rightarrow Mg$	3.7×10^{-10}	−0.86	6

O–H system

Reaction	A	$E_a[K]$	α	Ref.	Label
$H_2 + O \rightarrow H_2O$	1.0×10^{-16}	0	0	1	e
$OH + H \rightarrow H_2O$	1.0×10^{-16}	0	0	7	f
$O + O \rightarrow O_2$	1.0×10^{-18}	0	0	1	g
$OH + O \rightarrow O_2 + H$	2.0×10^{-7}	2795	−0.91	7	h
$OH + OH \rightarrow O + H_2O$	9.1×10^{-11}	3488	0	7	
$OH + OH \rightarrow O_2 + H_2$	2.8×10^{-11}	18 369	0	7	
$O + H \rightarrow OH$	1.1×10^{-19}	0	0.8	1	i
$H + OH \rightarrow O + H_2$	3.7×10^{-10}	6659	0	7	j
$OH + H_2 \rightarrow H + H_2O$	5.3×10^{-17}	1527	1.8	7	k

H^- system

$H + e^- \rightarrow H^-$	1.0×10^{-18}	0	1.0	2	
$H^- + H \rightarrow H_2 + e^-$	1.3×10^{-9}	0	0	2	

References

1 Estimate.
2 Prasad & Huntress (1980).
3 Millar (1980).
4 Turner & Dalgarno (1977).
5 Fahey *et al.* (1981).
6 Aldrovandi & Péquinot (1973).
7 Hardy *et al.* (1978).
8 Seaton (1951).

Table 2. Photodestruction reactions and rates.

Group	Reaction	Rate (C/S) [s^{-1}]	Rate (ISM) [s^{-1}]	Ref.	Label
III(G)	$SiH^+ + h\nu \rightarrow Si^+ + H$	2.0×10^{-5}	–	1	
I(C)	$SiO + h\nu \rightarrow Si + O$	6.1×10^{-7}	1.3×10^{-11}	1	l
I(D)	$SiO + h\nu \rightarrow SiO^+ + e^-$	3.0×10^{-7}	–	2	m
II(B)	$SiH + h\nu \rightarrow Si + H$	3.2×10^{-3}	1.3×10^{-10}	1	
III(B)	$SiH + h\nu \rightarrow SiH^+ + e^-$	2.0×10^{-5}	–	2	
III(H)	$SiH_2^+ + h\nu \rightarrow Si^+ + H_2$	2.0×10^{-4}	–	2	
I(A)	$SiO_2 + h\nu \rightarrow SiO + O$	5.3×10^{-5}	3.6×10^{-10}	3	
III(I)	$Si + h\nu \rightarrow Si^+ + e^-$	3.4×10^{-4}	1.3×10^{-9}	4	
–	$O_2 + h\nu \rightarrow O + O$	1.7×10^{-4}	2.7×10^{-10}	5	
–	$OH + h\nu \rightarrow O + H$	2.1×10^{-4}	–	6	n
–	$H_2O + h\nu \rightarrow OH + H$	3.5×10^{-4}	4.5×10^{-10}	7 8	o
–	$Mg + h\nu \rightarrow Mg^+ + e^-$	1.2×10^{-5}	1.6×10^{-11}	9	
–	$S + h\nu \rightarrow S^+ + e^-$	6.2×10^{-6}	3.5×10^{-10}	10	
–	$Na + h\nu \rightarrow Na^+ + e^-$	4.6×10^{-5}	1.1×10^{-11}	11	
–	$Ca + h\nu \rightarrow Ca^+ + e^-$	3.4×10^{-4}	1.2×10^{-10}	12, 13	
–	$H^- + h\nu \rightarrow H + e^-$	1.7×10^{4}	–	14	

Notes
Rate (C/S) is the rate for the flux $2R_*$ from α Ori.
Rate (ISM) is the rate for the Habing (1969) interstellar field.

References
1 See text and Table 3.
2 Estimate.
3 Inn *et al.* (1953).
4 Chapman & Henry (1972).
5 Okabe (1978).
6 van Dishoeck (1983, in preparation)
7 Tan *et al.* (1978).
8 Hudson (1971).
9 Dubau & Wells (1973).
10 Kelly (1972).
11 Hudson & Carter (1967a).
12 Carter, Hudson & Breig (1971).
13 Hudson & Carter (1967b).
14 Wishart (1979).

assumed to be highly reactive. Most of the ΔG values were taken from the JANAF Tables (1971) and supplements. For the ions SiH^+ and SiO^+, ΔG was calculated using molecular data taken from Huber & Herzberg (1979). For SiO_2, we took the experimental results of Brewer & Rosenblatt (1969): ΔH (SiO–O) = 4.7 eV. Pacansky & Hermann (1978) made an *ab-initio* study of SiO_2 and found that it is stable with respect to SiO + O, the bond

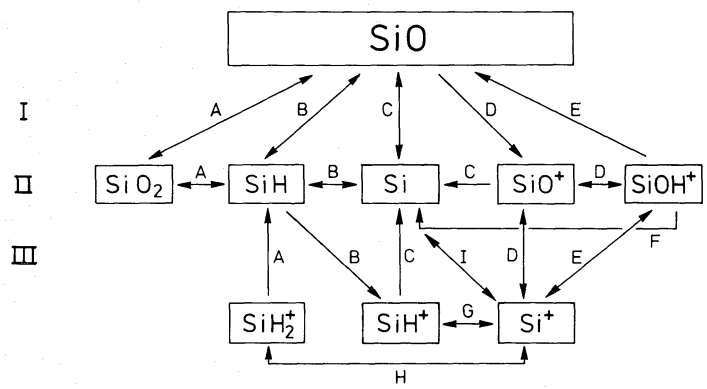

Figure 2. Network of reactions considered for silicon chemistry. The groups IA, etc., are referred to in Tables 1 and 2. Reactions of the O–H system are not shown here.

energy being 1.9 eV. We adopt the experimental value but regard it as uncertain by ± 0.5 eV. The heat of formation of $SiOH^+$ was taken from Fahey, Fehsenfeld & Ferguson (1981).

2.3 PHOTO-RATES

The photoioinzation and photodissociation rates were computed as

$$c \int_{912\,\text{Å}}^{\lambda_{th}} \sigma_\lambda \, n_\lambda \, d\lambda \, [s^{-1}] \tag{3}$$

where λ_{th} is the threshold wavelength for photoionization or dissociation, σ_λ is the wavelength dependent cross-section [cm^2] and n_λ the photon density [cm^{-3}] as deduced from the adopted flux curve in Fig. 1. Rates were also computed for the interstellar radiation field (Habing 1969), in part to provide a check on the method by enabling comparison with previously published rates. Results of the integrations are shown in Table 2. A major difference between C/S and interstellar photoreactions is that, in the former, threshold wavelengths play an important role because the UV flux drops rapidly at short wavelengths while in the latter the UV flux is relatively constant with wavelength. At any radius from the star the rate is scaled by the factor $(R/2R_*)^{-2}$, i.e., the assumption is made that the cool region is optically thin in the ultraviolet. This assumption is discussed in Section 5.

The interstellar UV field was also considered as a contributor to C/S photoreactions. It was found that, even for a cool star with only 1 per cent of the α Ori UV flux, at wavelengths longer than 1080 Å the C/S flux dominated out to a radius of $30R_*$ (2.1×10^{15} cm). Our calculations are restricted to $R < 30R_*$ because, at larger radii, the time-scale to reach steady-state concentrations becomes larger than the expansion time-scale; thus for $R > 30R_*$ the steady-state approximation is no longer valid. Integration of equation (3) was done using the smoothed curve shown in Fig. 1. A careful check was made to ensure that no resonance peaks in the absorption cross-sections coincided with strong emission lines in the α Ori spectrum.

For H^- photoabsorption we used a smoothed stellar flux curve derived from the *UBVRIJK* photometry of Johnson (1967). References for the photoabsorption cross-sections of H_2O, O_2, H^- and OH are given in Table 2. The cross-section for OH is from new calculations for the $^2\Sigma^- - X^2\Pi$ transition, and the resulting photodissociation rate for the Habing field is larger than previous estimates (van Dishoeck 1983, in preparation). The photodestruction of H_2, $SiOH^+$ and SiO^+ was not included. The C/S flux near the Lyman lines of H_2 is low, and these lines have large optical depth if H_2 is significantly associated. For $SiOH^+$ and SiO^+, it can be shown that photodissociation would proceed much more slowly than electron dissociative recombination. Photodissociation cross-sections for Si-bearing molecules have not been measured or calculated. For SiO_2 we took the measured CO_2 cross-sections (Inn, Watanabe & Zelikoff 1953) evaluated at wavelengths scaled by the ratio $D_0^0(CO-O)/D_0^0(SiO-O) = 5.45/4.7$. The threshold wavelength for SiO_2 photodissociation is then 1970 Å. Values for the cross-sections of SiO, SiH and SiH^+ were estimated using the relation:

$$\int_0^\infty \sigma_\nu \, d\nu = \frac{\pi e^2}{mc} f \tag{4}$$

where f is the oscillator strength of the transition producing the photodissociation. The integral in (4) was approximated by $\sigma_{max} \cdot \Delta\nu_{1/2}$ where $\Delta\nu_{1/2}$ is the width at half maximum of the absorption profile, which was assumed to be triangular. Table 3 shows the parameters

Table 3. Values of parameters used in the calculation of photodissociation cross-sections for SiH, SiH^+ and SiO.

Molecule	Transition	ν_{00} (cm^{-1})	$\Delta\nu$ (cm^{-1})	λ_{00} (Å)	f	σ_{max} (10^{-18} cm^2)
SiH	$B^2\Sigma^+$–$X^2\Pi$	34 388	8066	2908	0.004	1.0
	$D^2\Sigma^+$–$X^2\Pi$	52 247	8066	1914	0.005	2.3
	$E^2\Sigma^+$–$X^2\Pi$	43 744	8066	2286	0.01	1.1
SiH^+	$^1\Sigma^+$–$X^1\Sigma^+$	64 528	8066	1550	0.01	1.2
SiO	'Quasi- –$X^1\Sigma^+$ continuum'	85 000	5250	1176	0.01	1.8

adopted for the three molecules, now discussed briefly. (All molecular data were taken from Huber & Hertzberg 1979 unless otherwise noted.)

2.3.1 SiH

Predissociation has been reported from the $B^2\Sigma^+$ and $D^2\Delta$ states. Photodissociation was assumed to proceed by absorption from the $X^2\Pi$ ground state into one of these two states or into a repulsive $^2\Sigma^+$ state. Oscillator strengths for the first two transitions were assumed to be the same as for the corresponding transitions in CH given by Hinze, Lie & Liu (1975), while for the transition into the repulsive state we assumed $f = 0.01$.

2.3.2 SiH^+

There is no report of predissociation. By analogy with CH^+ (Saxon, Kirby & Liu 1980) we assumed that a weakly bound $^1\Sigma^+$ state with a potential maximum exists at an excitation energy of ~ 8 eV (outside the range of spectroscopic studies for this molecule). The transition into this state is also assumed to have an oscillator strength of $f = 0.01$ and to lead to dissociation.

2.3.3 SiO

There is no report of predissociation in the literature. According to theoretical studies by Robbe *et al.* (1979) and Heil & Schafer (1972) there is a large density of states, many repulsive, at ~ 10 eV above the ground state. We assume that absorption into the quasi-continuum produced by these states results in the photodissociation of the SiO molecule. Values of ν_{00} and $\Delta\nu_{1/2}$ were calculated by examining the region of overlap between the wavefunction of the $v = 0$ vibrational level of the ground state and a typical repulsive curve profile (i.e. using the Franck–Condon principle). The absorption profile is approximated as triangular and the central frequency is 85 000 cm^{-1} (λ = 1176 Å). This threshold wavelength is considerably shorter than that corresponding to the binding energy of 8.26 eV, namely λ = 1500 Å, and is close to the ionization potential (11.4 eV or 1087 Å). The C/S flux is low at 1176 Å and thus photodissociation of SiO is slow.

3 Results

The steady-state solution for the set of species and reactions listed in Tables 1 and 2 was found using a computer program developed by Drs Tielens and Hagen (Tielens 1982). The total gas density, kinetic temperature and radiation field determine the reaction rates. The

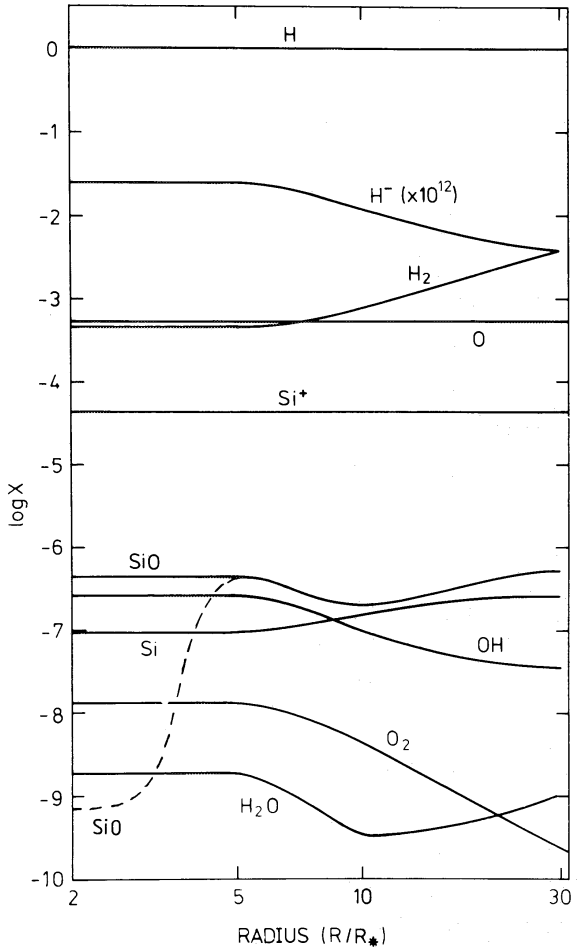

Figure 3. Composition of C/S gas at different distances from α Ori, for $\dot{M} = 2 \times 10^{-6} M_{\odot}\,\mathrm{yr}^{-1}$. $X = n(\text{molecule})/n(\text{total})$. At $R = 2R_*$, $n = 3 \times 10^9\,\mathrm{cm}^{-3}$ and $T = 1100\,\mathrm{K}$. The dashed line indicates the SiO concentration in a model where reactions with C^+ occur between 2 and $5R_*$ (see Section 6).

equations of constraint are derived from the zero net rate of change of all species concentrations, plus charge neutrality.

Results for the α Ori shell are shown in Fig. 3. The initial parameters used are $T_0 = 1100\,\mathrm{K}$, $R_0 = 2R_*$ and $n_0 = 3 \times 10^9\,\mathrm{cm}^{-3}$. The UV flux is given by the adopted flux curve (Fig. 1) and the temperature was varied as described above. Many abundances are constant with radius, presumably because in a shell which has a steady flow and is optically thin, both gas density and radiation field decrease as R^{-2}. Thus the competition between gas kinetic and photoreactions remains the same, except in so far as the former rates vary with temperature owing to the different activation energy barriers. A result which is surprising is that most of the silicon is in the form of Si^+ rather than SiO. The metals such as Fe, Mg and Na are mostly ionized, a result in agreement with that of Bernat (1977). The dominant reactions for the formation and destruction of the abundant molecules SiO, OH, O_2 and H_2O are given in Table 4. The predicted concentrations for the calculations in which E_a was taken to be zero for radical–molecule reactions were within a factor of 2 of those shown in Fig. 3.

Molecular ions were always found to have low abundances, as can be seen from Table 5. This result is due to their rapid rates for dissociative recombinations, typically $10^{-7}\,\mathrm{cm}^3\,\mathrm{s}^{-1}$, which are roughly 10^5 times faster than atomic recombination rates. If there is sufficient

Table 4. Dominant destruction and formation reactions for SiO, OH, O_2 and H_2O at 5, 10 and 30 R_*.

	SiO	OH	O_2	H_2O
5 R_*	a	i, j_{rev}	h	k
	l, m	j, n	h_{rev}, g_{rev}	d, o
10 R_*	a	b_{rev}, j_{rev}	c, h	e, f, k
	l, m	b, n	g_{rev}	d, o
30 R_*	a	i	c	e
	l, m	b, n	g_{rev}	d, o

Note
At each radius the upper row indicates the dominant formation reactions and the lower row, dominant destruction reactions. The letters refer to the labels shown in Table 2. 'rev' denotes a reverse reaction.

UV radiation to produce molecular ions, then the same radiation ionizes the metals, and the resulting photoelectrons can quickly neutralize the molecular ions. The net result of a high UV flux is therefore over-dissociation of molecules rather than over-ionization. These ions were nevertheless included because they may provide fast channels for cycling SiO

Table 5. Abundances and e-folding time-scales around α Ori at 2 and 30 R_*.

Species	log X (2 R_*)	T (2 R_*) [s]	log X (30 R_*)	T (30 R_*) [s]
e^-	−3.9	2.6×10^{5}	−3.9	9.5×10^{7}
H	0.0	9.6×10^{8}	0.0	2.7×10^{12}
H_2	−3.9	8.5×10^{5}	−2.4	5.7×10^{11}
O	−3.3	9.2×10^{5}	−3.3	1.0×10^{10}
Si	−7.0	2.9×10^{3}	−6.6	6.6×10^{5}
Na	−7.7	2.2×10^{4}	−7.2	4.9×10^{6}
Fe	−6.1	3.3×10^{4}	−5.6	7.5×10^{6}
Mg	−5.9	8.3×10^{4}	−5.3	1.9×10^{7}
S	−5.8	1.6×10^{5}	−5.4	3.6×10^{7}
Ca	−8.6	2.9×10^{3}	−8.0	6.6×10^{5}
Si^+	−4.4	7.6×10^{5}	−4.4	1.1×10^{8}
Na^+	−5.7	2.3×10^{6}	−5.7	1.6×10^{8}
Fe^+	−4.4	1.6×10^{6}	−4.4	1.2×10^{8}
Mg^+	−4.4	2.9×10^{6}	−4.4	1.5×10^{8}
S^+	−4.8	1.5×10^{6}	−4.9	1.2×10^{8}
Ca^+	−5.7	2.3×10^{6}	−5.7	1.6×10^{8}
SiO	−6.4	1.1×10^{6}	−6.3	2.5×10^{8}
SiO^+	−10.0	3.8×10^{0}	−9.9	5.6×10^{3}
SiH	−11.0	1.2×10^{2}	−9.8	7.0×10^{4}
SiH^+	−12.3	3.3×10^{-1}	−12.4	7.5×10^{1}
SiO_2	−14.0	1.0×10^{2}	−18.7	4.2×10^{6}
$SiOH^+$	−11.6	4.3×10^{0}	−11.5	1.0×10^{3}
SiH_2^+	−12.5	5.2×10^{0}	−11.5	1.2×10^{3}
OH	−6.7	3.3×10^{2}	−7.4	6.7×10^{5}
O_2	−7.9	1.5×10^{3}	−9.6	1.3×10^{6}
H_2O	−8.7	1.5×10^{3}	−9.0	3.5×10^{5}
H^-	−13.6	5.9×10^{-5}	−14.4	1.3×10^{-2}
Expansion time		1.4×10^{9}	–	2.1×10^{10}

molecules. For example, around α Ori an important formation route for SiO is dissociative recombination of $SiOH^+$.

Results for a cooler star which has only 1 per cent of the flux of α Ori were also computed. Because of the reduced radiation field, fuller molecular association was achieved. The Si-atoms were almost all bound up in the SiO molecule, while the remaining oxygen is contained in water molecules. However, in this case, a self-consistent model is not achieved because the continuum optical depth is large, and detailed modelling of the radiative transfer through the shell would be required. These optical depth effects are discussed further in Section 5.

The variation of the molecular concentrations with UV flux is shown in Fig. 4. It should be noted that the inverse of this behaviour represents the density dependence, because a factor of 10 increase in density mimics quite well the same factor decrease in flux. The chemical equilibrium around stars with high UV flux like α Ori is not temperature-sensitive (Fig. 2) because the UV field controls many abundances. Hence, our ignorance of the gas temperature is not critical. However, the solution for $F_\lambda = 0.01 F_{std}$ is more temperature-sensitive because here, collisions are important, and the chemical equilibrium is determined by the β and ΔG values. As the ultraviolet flux tends to zero, the solution tends to the thermodynamic equilibrium limit. Since Jura & Morris (1981) have recently argued that

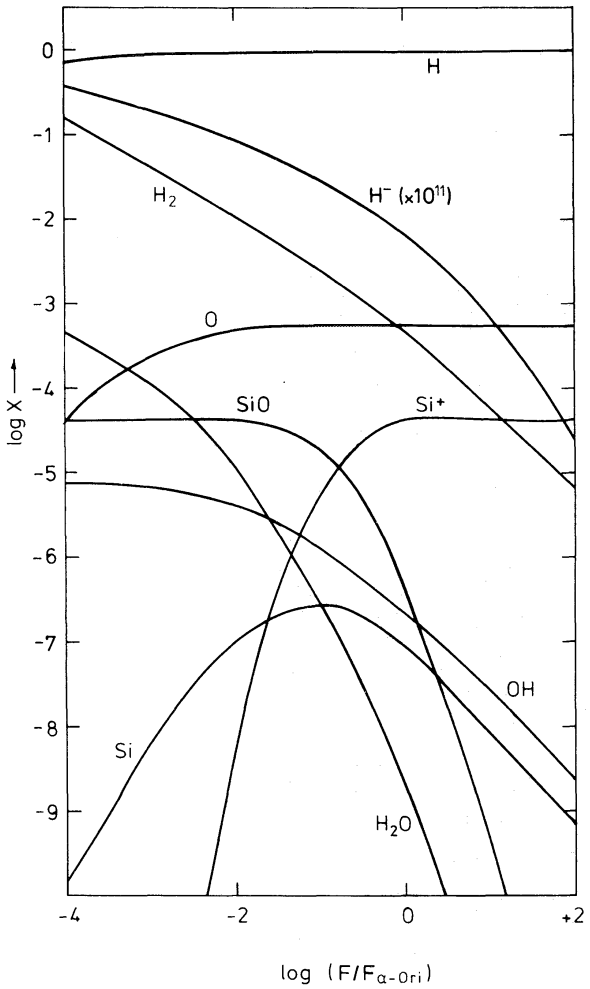

Figure 4. Variation of predicted C/S gas composition with UV flux level. The reference level is the measured α Ori flux. The temperature and density used are those for $2R_*$ from α Ori.

$\dot{M}$ for α Ori is $1.5 \times 10^{-5}\, M_\odot\, \mathrm{yr}^{-1}$, a factor of 7 larger than the rate adopted as our standard, we computed the steady-state solution for this value of $\dot{M}$ as well. The main changes can be read from Fig. 4 for the case $\log (F/F\alpha\,\mathrm{Ori}) \simeq -0.9$ since the UV flux decrease mimics the gas density increase as noted above. In particular, note that SiO, OH and H_2O will have significantly higher concentrations. As a result, optical depths in the photoabsorption continua of SiO and OH will become greater than order one and again radiative transfer models are required for precise solutions.

4 The H/H_2 ratio

Fig. 4 shows that hydrogen is predicted to be mostly in atomic form, i.e. $n(H) > n(H_2)$, even when the UV flux is only 1 per cent of the α Ori value. This result is due to a shift in the chemical balance: molecules such as OH and H_2O are dissociated, and they affect the H–H_2 system through several of the reactions listed under the 'O–H system' in Table 1. Inclusion of H_2 dissociation via the Lyman band lines would increase the tendency towards atomic H still further.

For the model to be valid, chemical time-scales must be less than the expansion time-scale $\Delta R/v_e$. The characteristic length scale ΔR is taken to be 2×10^{14} cm, i.e. the distance between 2 and $5R_*$. The time-scales involved (Table 5) suggest that further study of the H/H_2 ratio in our calculations is warranted. This ratio is not fixed as an input parameter but is found as a part of the solution of the steady-state equations. A discussion of the time-scale for conversion of atomic to molecular hydrogen was given by Clegg & Wootten (1980). The three-body reaction $H + H + H \rightarrow H_2 + H$ was not included in the present set because the time-scale for H consumption $T(H) = (k n_H^2)^{-1} \geqslant 2 \times 10^{12}$ s. The transference from H to H_2 can occur, however, via H^- ($H^- + H \rightarrow H_2 + e^-$) or via reactions involving OH, O and H_2O (Table 1, OH system). Formation of H_2 via H^- is slow because of the low H^- steady-state concentration, which is a result of the rapid photodetachment by the high photon flux in the visible and near-IR.

At $T = 1000$ K the most rapid conversion to H_2 occurs via

$$OH + H \rightleftarrows O + H_2$$

for which $T(H) = 2 \times 10^9$ s, a time just consistent with the steady-state assumption. At lower temperatures, however, $T(H)$ increases because of the activation energies of these reactions and, as a result, the H/H_2 ratio is effectively frozen for $T < 700$ K at a density of $3 \times 10^9\ \mathrm{cm}^{-3}$. Because the H–$H_2$ system only just satisfies the steady-state approximation, we need to consider whether the gas arriving in the cool region may have a quite different H/H_2 ratio. This gas must flow from the stellar photosphere through the chromosphere. In the photosphere at the temperature minimum ($T = 2700$ K) the pressure-dependent ratio $n(H)/n(H_2) = 3 \times 10^2$ at $P = 5$ dyne/cm^2 and 50 at $P = 30$ dyne/cm^2. Model atmospheres for red giants (Johnson, Bernat & Krupp 1980) with $T_{\mathrm{eff}} = 3800$ K and $\log g = 0.0$–1.0 have gas pressures at small optical depth ($\tau_{1\mu} = 10^{-4}$) in this range. Thus H_2 molecules are not expected to be highly associated in the outer layers of the photosphere. In the α Ori chromosphere the temperature is expected to be 5000–7000 K (Basri *et al.* 1981) and the concentration of molecular hydrogen will be very low. Therefore the gas entering the cool region will be mostly atomic H.

To demonstrate the importance of the H/H_2 ratio we show in Fig. 5 the results of calculations made with artificially-imposed H/H_2 ratios. The solution was obtained for the parameter values appropriate for $R = 2R_*$ from α Ori. The high cosmic abundance of H provides the reason for the importance of this ratio.

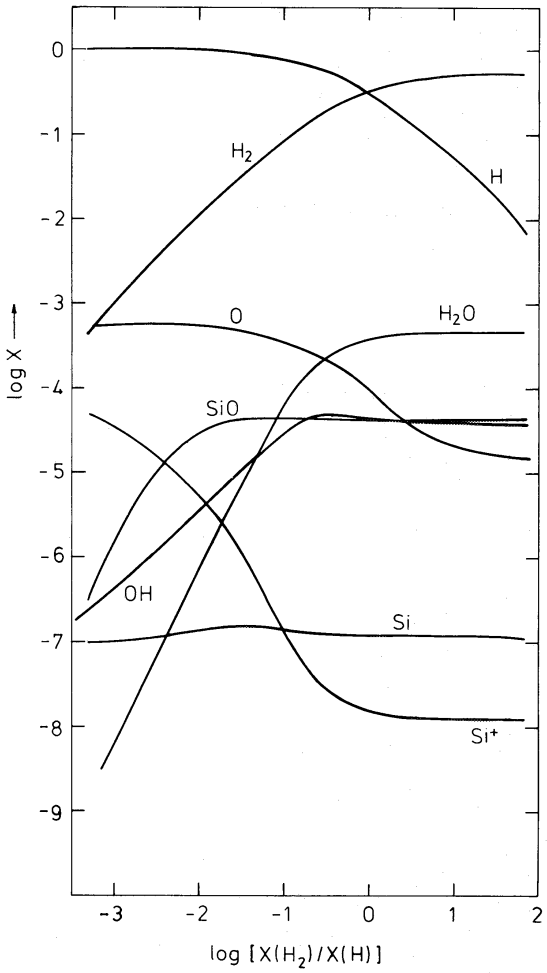

Figure 5. Variation of predicted C/S gas composition with (artificially imposed) ratio of atomic to molecular hydrogen. Temperature and density used are those for $2R_*$ from α Ori.

5 Discussion of physical processes

We are able to deduce some simple results about time-scales, continuum optical depths and photo-electron heating rates in the cool region. These quantities may be calculated once the steady-state concentrations at each radius are known.

Table 5 shows the e-folding time-scale for each species, defined by the relation $T(X) = n(X)/\dot{n}(X)$ for species X where n and $\dot{n}$ are the density [cm^{-3}] and its total time derivative, respective. T has been evaluated for the α Ori shell at radii of 2 and $30R_*$; the values should be compared with the expansion time $T_{exp} = R/v$, also listed in the table.

The result is that the steady-state assumption is valid for all species at $R = 2R_*$ but invalid for H, H_2 and O at $30R_*$ because of the reduced temperature and density. For the case of the stars with lower UV flux, the steady-state assumption breaks down at smaller radii, with H, H_2, O, S and SiO having $T > T_{exp}$ at $15R_*$ in the optically-thin case, and at even smaller radii if the UV continuum optical depth is allowed for.

In our calculations we assumed that the continuum optical depth $\tau < 1$, which permitted use of the formula $F_\lambda = F(R = 2R_*) \times (R/2R_*)^{-2}$ between 2 and $30R_*$. The optical depth for each species was computed using the formula.

$$\tau_i(\lambda) = \sigma_i(\lambda) \int_{2R_*}^{10R_*} n_i(R)\, dR$$

where σ_i is the photoabsorption cross-section for species i and $n_i(R)$ the density of the absorber at radius R. τ has been calculated at various wavelengths for the bound–free continuua represented by the photodissociation and photoionization reactions listed in Table 2. For atomic photoionization processes the value of τ at the threshold wavelength is shown in Table 6, and for Fe and Ca the value at a resonance peak in the absorption cross-section is also listed. For molecules, τ is evaluated at a wavelength where the cross-section is largest.

Inspection of Table 6 shows that 'optically-thin' assumption is just achieved for the α Ori case. Exceptions the C I and CO absorption continua; these are discussed in Section 6 below. For a star with a chromosphere weaker than that of α Orionis, optical depths can be considerably larger than unity: for example, for the case $F_\lambda = 0.01 F_{std}$, optical depths of 13, 56 and 69 are achieved for Fe I, S I and H_2O respectively. Consequently, the composition of the gas as a function of radius cannot be approximated by our model. In the optically-thick case the radiative transfer and chemistry are intimately coupled and highly detailed models would be required. In such models, molecular bound–bound transitions should also be considered. CO is likely to be a significant opacity source; it has several allowed transitions from the ground state between 980 and 1150 Å.

Some remarks on the τ values presented are pertinent. For the bound–free continua of neutral atoms, the radiation field is not reduced in proportion to $\exp(-\tau)$ because absorptions are balanced by emission from electron recombination. For H, He and O approximately 36 per cent of recombinations occur directly to the ground state (Allen 1973); the remaining 64 per cent produce photons in longer-wavelength continua which can escape from the shell. Hence, the radiation field is reduced by the factor $\exp(-0.64\tau)$ for such atomic bound–free continua.

For molecules, bound–bound and photodissociation transitions occur. The bound–bound transitions will complicate the transfer of radiation in the UV; the gas density is so low that lines form by scattering and the main effect on the spherically symmetric radiation field will be the redistribution of flux within certain wavelength regions corresponding to the effective width of the various electronic transitions. For the molecular photodissociation continua the reduction factor should indeed be $\exp(-\tau)$, because the inverse process which results in emission (radiative association) does not balance the photon absorption rate.

Table 6. Shell optical depths in bound–free continua at threshold and peak wavelengths.

Species	λ_{th} [Å]	$\tau(\lambda_{thr})$	λ_{peak} [Å]	$\tau(\lambda_p)$
Fe	1568	6.0×10^{-1}	1021	5.4
Na	2412	$8.\times10^{-4}$	–	–
Mg	1622	4.6×10^{-1}	–	–
Ca	2028	1×10^{-3}	1886	2.0×10^{-2}
Si	1521	1.2	–	–
S	1197	6.7	–	–
H^-	–	–	8500	3.0×10^{-7}
H_2O	2063	1×10^{-3}	952	1.5×10^{-2}
OH	–	–	1744	2.0×10^{-1}
SiO_2	–	–	1250	1.5×10^{-7}
O_2	–	–	1450	7.0×10^{-2}
SiO	–	–	1176	2.0×10^{-1}
SiH	–	–	2908	3.0×10^{-6}
CO	–	–	1050	4.9×10^{1}
C	–	–	1099	1.2×10^{3}

The main absorber below 1521 Å is Si I, while S I absorbs strongly below 1197 Å. If S atoms were bound in molecules (not considered in this programme) this opacity would be reduced. An LTE calculation for the case $n = 3 \times 10^9\,\mathrm{cm}^{-3}$ and $T = 1100\,\mathrm{K}$ was carried out which predicted that S is depleted in H_2S and SiS, but a detailed study would be needed to investigate S chemistry fully.

The increase in optical depths for the low UV-flux case is caused by a shift in the chemical balance towards neutral metal atoms and towards molecular association. Metal ions and neutral oxygen (a molecular dissociation product) have no continuum absorption longward of the Lyman limit. In other words, a high UV flux destroys the opacity which might have absorbed it, as also occurs in an H II region. An interesting consequence of this is that, for a stellar sequence in which the chromospheric UV flux decreases, the UV flux escaping from the shell would decrease sharply because of this chemical balance shift.

The absorption of UV photons leads to heating of the gas by hot photoelectrons, because recombining electrons have only the thermal energy $E \sim 0.1$ eV. Our steady-state results give the heating rate, once the average photo-electron energy in a photoabsorption continuum has been calculated. We computed the heating rates per unit volume at distances 2 and $5R_*$ from α Ori. The rates are 2.4×10^{-12} and $2.4 \times 10^{-14}\,\mathrm{erg\,cm^{-3}\,s^{-1}}$, respectively. These rates should be compared with the adiabatic cooling rate $p\,d\rho/\rho\,dt$ which equals 1.6×10^{-12} erg cm^{-3} s^{-1} at $2R_*$ and 6.4×10^{-14} at $5R_*$. Photoelectric heating is significant, and should be included in detailed shell models. A major heating source is the photodissociation of OH; although no photoelectron is involved, net heating is provided because the transition occurs via a repulsive state in OH.

6 Silicate grain formation

Our results imply that for α Ori at $2R_*$, a gas density of about $10^{11}\,\mathrm{cm}^{-3}$ is required for SiO to be significantly associated. Since α Ori has an IR excess and a silicate emission feature at 9.7 μm (Dyck & Simon 1975), the question arises then, in view of the high calculated abundance of Si^+, as to whether SiO molecules in the gas phase are a prerequisite for nucleation of silicate grains. A discussion of this point is beyond the scope of this paper. However, we point out that one theory of grain condensation – ionic nucleation (e.g., Tabak *et al.* 1975) – actually requires the presence of some ions.

Another possibility is that SiO_2 may be an important intermediate in silicate grain formation. We have examined the likely abundance in the C/S gas, and found that SiO_2 never contains a significant fraction of the available silicon atoms. Our estimated value of $D_0^0(SiO_2)$ was raised by 1.0 eV in one calculation, and while a factor 200 increase in its abundance at 1100 K was noted, it still contained less than 2 per cent of Si atoms.

If gaseous SiO molecules *are* required for silicate grain formation, then an ultraviolet flux will inhibit this process near a stellar chromosphere. This could provide the explanation of why grains have so far only been observed at several stellar radii away from α Ori, as described in the Introduction. The concentration of SiO is low at radius $2R_*$ but can increase near $R = 5$–$10R_*$ as optical depth builds up in the S I continuum shortward of 1197 Å (see Table 6). Observations of C/S SiO absorption lines and of dust emission closer to the star are needed to settle this question.

7 The C^+–CO system

After our calculations for Si chemistry were completed, we extended our reaction set to include C, C^+ and CO. Photoabsorption cross-sections of C I and CO were taken from

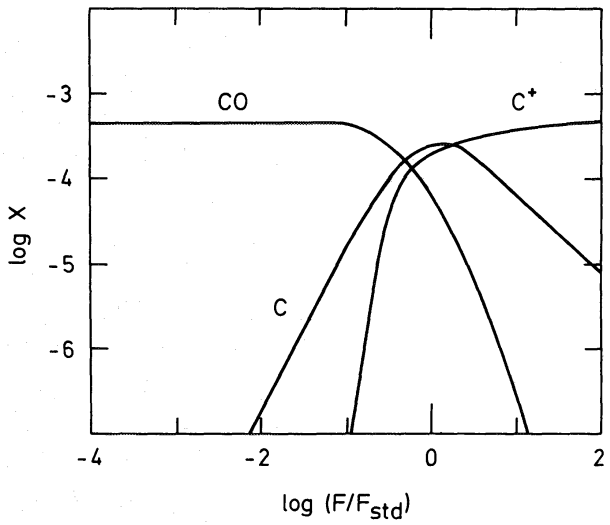

Figure 6. Solution for the predicted concentrations of C, C^+ and CO at a distance $2R_*$ from α Orionis. The concentrations are given as a function of UV flux level, as in Fig. 4. The calculations are described in Section 6.

Hoffman & Trefftz (1980) and Solomon & Klemperer (1972) respectively. The C^+ recombination coefficient was from Prasad & Huntress (1980). Reactions between C atoms and the molecules OH, H_2O, SiO and O_2 were taken to have the rate $5 \times 10^{-11} \exp(-1000/T)\,\mathrm{cm^3\,s^{-1}}$. Reverse reactions were included, as were reactions between C^+ and SiO and between C and SiO^+ (Prasad & Huntress 1980).

The predicted concentrations of C, C^+ and CO as a function of the UV flux are shown in Fig. 6. The density and temperature are those for the point at $2R_*$ from α Orionis, as in Fig. 4. CO is not fully associated for the case $F = F_{\mathrm{std}}$, but calculation of the optical depths in the C I and CO absorption continua shows that they are quite optically thick. The optical depths were given in Table 6. The radiation field from α Ori will quickly be attenuated for wavelengths below 1099 Å (the C I photoionization threshold) and almost all C atoms will be in the form of CO, as described in Fig. 6, at a few stellar radii from the star.

This conclusion does not conflict with the observed α Ori UV flux level, because the observations only extend to about 1200 Å. While calculation of the SiO dissociation rate involves only a short extrapolation to 1176 Å, extrapolation to 1099 Å is less certain. Our conclusion is that the CO seen in the expanding shell around α Ori should contain nearly all the C atoms. (Far from the star, the interstellar UV radiation may dissociate the CO.) The CO $J = 2-1$ observations have been discussed by Knapp *et al.* (1980) and by Jura & Morris (1981).

Reactions between C^+ and SiO affect the concentration of SiO considerably, while predicted values of $n(\mathrm{Si})$ and $n(\mathrm{Si^+})$ are scarcely affected. In Fig. 3 the dashed line shows the SiO concentration for a calculation in which the carbon system just described was included, but only for $R < 5R_*$. For $R > 5R_*$ it was assumed that all C would be in CO because of the large C I and CO optical depths.

8 The SiO maser

SiO maser emission occurs from the $v = 1$, 2 and 3 vibrational levels of the $X^1\Sigma^+$ ground state. The emission is seen from O-rich luminous cool stars of spectral type M3 or later, and from two S-type stars, χ Cyg and W And which both have only mild S-characteristics. No

maser emission has been detected from α Ori. VLBI results have shown that the emission must be located close to the star. For example, for R Cas (M6–M8 Mira variable) and VX Sgr (M5 supergiant) the 'true' masing–volume radii were found to be 2×10^{14} and 1.5×10^{15} cm respectively, while the stellar radii are 3×10^{13} and 10^{14} cm (Moran *et al.* 1979). The average photon emission rate in a strong line such as the $v = 1$, $J = 1 \rightarrow 0$ transition is $\Phi = 2 \times 10^{43}\ s^{-1}$ (Spencer *et al.* 1981) but in strong sources such as R Leo we calculate $\Phi = 1 \times 10^{44}\ s^{-1}$.

Although Elitzur (1980) has proposed a model in which the SiO maser is located within the stellar atmosphere and is pumped by collisions with H or H_2, it is worthwhile to consider the possibility that the maser is located in the 'cool region' which we have studied here. Most reactions which form SiO will produce it vibrationally excited. An example of this mechanism is given by Hager, Harris & Hadley (1974) who reported SiO $^3\Pi$–$X^1\Sigma^+_i$ and $^3\Sigma$–$X^1\Sigma$ chemiluminescence produced by the reaction $Si + N_2O \rightarrow SiO + N_2$. Significant population of the $v = 1$ and 2 levels of the triplet state was observed. Other chemiluminescent studies show that SiO can be formed in the $A^1\Pi$ state from the reaction of $SiCl_4$ and oxygen atoms (Shanker, Linton & Verma 1976). The SiO ($A^1\Pi$) molecules were formed with a high degree of vibrational excitation (up to $v = 10$) but without high rotational excitation. The reactions included in our program which form SiO have not been observed in the laboratory. However, we have checked that formation of SiO ($A^1\Pi$) is allowed by spin and molecular orbital symmetry conservation rules for reactions between ground state Si and OH or O_2. Once SiO has formed in this state, the predominant relaxation channel is fluorescence to the $X^1\Sigma^+$ ground state. The expected population of the vibrational levels in the $X^1\Sigma^+$ state have been calculated using Franck–Condon factors (Liszt & Smith 1972) and are listed in Table 7. The $A^1\Pi$ state is assumed to be formed with $T_{vib} = 2500$ K. Significant population of the $v = 1$, 2 and 3 levels occurs, just the levels from which maser emission is observed.

In this scheme, chemical reactions populate the excited vibrational levels, but the inversion is still produced by optical depth effects in the fundamental SiO lines near 8 μm, as in the model Elitzur (1980). To produce the observed photon emission rate, each SiO molecule must be destroyed and reformed many times in the circumstellar flow. This requirement can be demonstrated by calculating the rate of loss of Si atoms from a star having $\dot{M} = 10^{-6} M_\odot\ yr^{-1}$; the rate is $1.5 \times 10^{39}\ s^{-1}$ (with adopted cosmic abundance $A(Si) = 7.6$). This rate is four orders of magnitude less than the masing photon emission rate of 10^{43}–$10^{44}\ s^{-1}$.

One prerequisite for a population inversion to occur in a level such as $X^1\Sigma^+$, $v = 1$ is that $nk_{1,0} < A_{1,0}$ where $k_{1,0}$ is the vibrational collisional de-excitation rate for $v = 1 \rightarrow 0$ for SiO, n is the density of H or H_2 and $A_{1,0}$ the transition rate for the $v = 1 \rightarrow 0$ band. This requirement translates into $n < 10^{10}\ cm^{-3}$, but Elitzur (1980) proposed that, for the collisional pump model, the gas density could be as high as $10^{12}\ cm^{-3}$. Bujarrabal & Rieu (1981) show that maximum maser emission would occur at $n = 10^{11}\ cm^{-3}$. We have examined the total rate of formation of SiO molecules for the case $n = 10^{11}\ cm^{-3}$, $T = 1100$ K and UV flux levels between 10^{-3} and 10 times the α Ori value. The largest production rate, $91\ cm^{-3}\ s^{-1}$ occurred for a UV flux of 1 per cent of the standard value, although it was not strongly

Table 7. Vibrational state population (in percent) of SiO ($X^1\Sigma$) after relaxation from $A^1\Pi$ at 2500 K.

v''	0	1	2	3	4	5	9
Pop.	19.2	17.6	15.0	12.6	10.2	8.2	4.0

flux-dependent or sensitive to the addition of the carbon-system to the main reaction set. The volume required to produce the observed emission rate may be computed approximately from an adaption of Elitzur's equation (32):

$$\Phi = \frac{R(\mathrm{SiO})\,X_0\,V}{[1+J(C_{10}/\Gamma)]}$$

where $R(\mathrm{SiO})$ is the formation rate of SiO, X_0 the fraction of molecules in the $v=0, J=0$ level and V is the emitting volume. The term in brackets gives a correction for collisional de-excitation of the $v=1$ level. C_{10} is the rate for this with H or H_2 as collision partner and $\Gamma = 2A_{10}/(2J+1)\tau$ where τ is the optical depth in the fundamental band P(1) line. Elitzur estimates the term in brackets to be 10. Note that we neglected collisional excitation; in our scheme the temperature may be arbitrarily low and thus the rate for this quite slow.

With the data from Table 7 and an assumed rotational temperature $T_{\mathrm{rot}} = 1000\,\mathrm{K}$, which corresponds to a partition function $Q_{\mathrm{rot}} = 1047$, we find $X_0 = 1.8 \times 10^{-4}$. Thus a spherical emitting volume of radius 2.3×10^{15} cm would be required to produce 10^{44} photons s^{-1}. This is larger by factors of 1.5–10 than the radii measured from the VLBI experiments. This failure of the chemical maser model results from the stability of the SiO molecule, which is difficult to dissociate, and the low abundance of the reactants OH, O_2 and SiO_2 compared to the abundance of H or H_2. Note that, in this model and that of Elitzur, the pump rate per unit volume is proportional to the square of the gas density. In radiative pump models the density dependence is only linear.

Two ways in which the chemical pump rate might be increased are now briefly considered. First, significant cycling of SiO took place via the reactions between SiO_2 and H or H_2. If most of the silicon were contained in SiO_2 at some point in the C/S shell before silicate grains condense, the rate of formation of SiO from these latter reactions could in principle be quite high; but, as noted in Section 6, SiO_2 is not predicted to be abundant. Secondly, note that the pump rate is proportional to T_{rot}^{-1} through the dependence on X_0. If SiO forms only in low rotational levels, as observed by Shanker *et al.*, could the pump rate be sufficiently enhanced? Because the SiO production rate, $91\,\mathrm{cm}^{-3}\,\mathrm{s}^{-1}$, is considerably slower than the vibration–rotation radiative decay rate ($n_{\mathrm{SiO}} A_{1,0} \sim 10^6\,\mathrm{cm}^{-3}\,\mathrm{s}^{-1}$) or the collisional redistribution rate ($k_{\mathrm{rot}} n_{\mathrm{H_2}} \sim 10^6\,\mathrm{cm}^{-3}\,\mathrm{s}^{-1}$) a significant amount of rotational excitation is expected between chemical reactions. Thus the pump rate is not likely to be increased much above our estimate.

Two radiative processes which might affect the SiO populations are absorption in the $A^1\Pi$–$X^1\Sigma^+$ band near 2360 Å and absorption of Lyman α radiation within the P–X band. Although the optical depth in the A–X transition is large, the flux near 2360 Å from the cool stars which have maser emission is likely to be low. Even for α Ori the effective flux at $2R_*$ for a 30 Å wide absorption band is $\sim 3 \times 10^{13}$ photons $\mathrm{cm}^{-2}\,\mathrm{s}^{-1}$, two orders of magnitude below the maser flux at $2R_*$ which is $\sim 3 \times 10^{15}$ photons $\mathrm{cm}^{-2}\,\mathrm{s}^{-1}$. However, the high optical depths in the A–X lines could provide a distortion of the rotational and vibrational level populations. High-resolution spectra of maser sources in the 2300 Å region would be useful to probe this possibility. Finally, we have examined the coincidence between the Ly α line and a part of the SiO P–X band (see Lagerqvist & Renhorn 1974). *Copernicus* spectra of cool giants (McClintock *et al.* 1975) show that the Ly α line will not be sufficiently broad to overlap with lines from low J-levels of the P–X band, whose origin is at 1220 Å. Thus distortion of SiO low J-levels by Ly α pumping will not occur.

Although the chemical pump model fails, the possibility that the maser is located in the cool region should be considered further (e.g., in radiative pump models). The low expansion

velocity of such a region provides a high gas density (for optical depth in the IR lines) and is consistent with the observed relation between maser and stellar velocities.

6 Concluding remarks

In this paper we have studied some of the physical and chemical processes which will occur in the layer of gas between a cool star and its expanding shell. The layer is really an extended stellar chromosphere: it is optically thin in the visible-wavelength continuum but not in resonance lines or in the far UV. Heating of such a region may occur via magnetic or acoustic waves, photoelectrons and in some cases molecular lines (see Goldreich & Scoville 1976). Cooling occurs by adiabatic expansion and line radiation.

We have shown that the UV chromospheric radiation illuminating such a cool region has a drastic effect on the chemistry. Molecular association is inhibited, and photoelectric heating is significant. The grain-forming gas around α Orionis contains many ions, including Si^+. The α Ori gas shell is just optically thin, but stars having lower chromospheric UV fluxes with similar mass-loss rates will have optically thick shells. For these, a detailed model would be needed which would solve the radiative transfer and chemical balance equations simultaneously.

We conclude by examining three types of observations which might provide diagnostics of the cool region. Infrared interferometry at 11 μm has already provided some results on the radial concentration of dust grains (discussed in Section 1). Improved interferometry at shorter wavelengths could give information on the distribution of warmer grains in the region between, say, $3-10R_*$ (Draine 1980). These observations will be difficult because at wavelengths shorter than 11 μm the ratio of flux emitted by grains to stellar flux is decreased, and because $10R_*$ corresponds only to 0.23 arcsec.

Secondly, high-resolution spectroscopy of the SiO fundamental lines near 8 μm would be valuable. The high optical depth of the $\Delta v = 1$ lines, relative to the 4 μm $\Delta v = 2$ lines, should ensure that a circumstellar component in the SiO is seen. Only the region interior to the point of significant silicate grain formation would contribute to these lines. The 8 μm lines have been studied toward VY CMa (Geballe, Lacy & Beck 1979), and laboratory measurements of these lines have recently been published (Lovas, Maki & Olson 1981). A resolution of $< 3\,\mathrm{km\,s^{-1}}$ ($\Delta\lambda/\lambda > 10^5$) is desirable in this case, especially since the cool region has such a low net expansion velocity. Thirdly, we consider fluorescent emission lines from molecules which could provide diagnostic information on the C/S chemistry and UV radiation field. A molecule may often be formed in an excited electronic state. De-excitation and stabilization occurs by a radiative transition to the ground state unless the transition is forbidden. Metastable states may also decay radiatively if the gas density is less than about $10^9\,\mathrm{cm^{-3}}$ (for a typical radiative lifetime of ~ 1 s). Such chemiluminescent emission lines may be distinguishable from their photospheric absorption line counterparts by either their narrower width or by a velocity shift. Two examples are given here. In the chemical maser model SiO is formed in the $A^1\Pi$ state. An observational test exists: if the model were successful, at least 10^{44} photons $\mathrm{s^{-1}}$ would be emitted in the A–X band from the whole shell. The resulting flux at Earth, for a star 100 pc distant and an effective A–X bandwidth of 50 Å, would be $1.4 \times 10^{-11}\,\mathrm{erg\,cm^{-2}\,s^{-1}\,\AA^{-1}}$. This would be easily detectable by the *IUE* satellite, although a shell optical depth of only 6 at 2360 Å would render the emission undetectable.

A second example is OH ($A^2\Sigma^+ - X^2\Pi_i$) emission near 3100 Å resulting from H_2O photodissociation. The quantum yield for OH emission is approximately 10 per cent for H_2O photoabsorption between 1100 and 1350 Å (Lee 1980). Our calculations show that, for the

entire shell between 2 and $5R_*$ around α Ori, the rate of H_2O photodissociation is too low by several orders of magnitude for the resulting OH A–X emission to be detectable by *IUE*. Monitoring of these bands in O-rich Mira variables might be useful, however, as a probe of the UV radiation emitted by the shocked gas in the outer layers of the photosphere. The structure of the layers of H_2O and OH molecules in relation to the pulsating star and its shock wave were demonstrated for R Leo by Hinkle (1978). Chemiluminescent emission from AlH molecules forming in such photospheres has been detected (Herbig 1956), and calculations suggest that, for gas densities greater than about 10^{13} cm^{-3}, detectable OH A–X emission would result from the dissociation of 10 per cent of H_2O molecules over a 10-day period. The OH band could be monitored by the *IUE* satellite.

Acknowledgments

We are grateful to Hans Olofsson and several colleagues in Leiden for useful discussions. RESC was supported by the Netherlands Foundation for Pure Science, ZWO.

References

Aldrovandi, S. M. V. & Péquignot, D., 1973. *Astr. Astrophys.*, **25**, 137.
Allen, C. W., 1973. *Astrophysical Quantities*, 3rd edn. The Athlone Press, London.
Basri, G. S., Linsky, J. L. & Eriksson, K., 1981. *Astrophys. J.*, **251**, 162.
Bernat, A. P., Hall, D. N. B., Hinkle, K. H. & Ridgway, S. T., 1979. *Astrophys. J.*, **233**, L135.
Bernat, A. P., 1977. *Astrophys. J.*, **213**, 756.
Bernat, A. P. & Lambert, D. L., 1976. *Astrophys. J.*, **204**, 830.
Brewer, L. & Rosenblatt, G., 1969. *Advances in High Temperature Chemistry*, Vol. 2, Academic Press, New York.
Bujarrabal, V. & Rieu, N. G., 1981. *Astr. Astrophys.*, **102**, 65.
Carter, V. L., Hudson, R. D. & Breig, E. L., 1971. *Phys. Rev. A.*, **4**, 821.
Chapman, R. D. & Henry, R. J. W., 1972. *Astrophys. J.*, **173**, 243.
Clegg, R. E. S. & Wootten, H. A., 1980. *Astrophys. J.*, **240**, 828.
Draine, B. T., 1980. In *Physical Processes in Red Giants*, eds Iben, I. & Renzini, A., Reidel, Dordrecht, Holland.
Dubau, J. & Wells, J., 1973. *J. Phys. B*, **6**, L31.
Van Duinen, R. J., Aalders, J. W. G., Wesselius, P. W. R., Wildeman, K. J., Wu, C. C., Luinge, W. & Snel, D., 1975. *Astr. Astrophys.*, **39**, 159.
Dyck, H. M. & Simon, T., 1975. *Astrophys. J.*, **195**, 689.
Elitzur, M., 1980. *Astrophys. J.*, **240**, 553.
Fahey, D. W., Fehsenfeld, F. C., Ferguson, E. E., 1981. *J. Chem. Phys.*, **75**, 669.
Geballe, T. R., Lacy, J. H. & Beck, S. C., 1979. *Astrophys. J.*, **230**, L47.
Gericke, K. H., Ortgies, G. & Comes, F. J., 1980. *Chem. Phys. Lett.*, **69**, 156.
Goldreich, P. & Scoville, N., 1976. *Astrophys. J.*, **205**, 144.
Habing, H. J., 1969. *Bull. astr. Inst. Netherlands*, **19**, 421.
Hager, G., Harris, R. & Hadley, S. G., 1974. *J. Chem. Phys.*, **63**, 2810.
Hardy, J. E., Gardiner, W. C. & Burcat, A., 1978. *Int. Jour. Chem. Kinetics*, **10**, 503.
Heil, T. G. & Schaefer, H. F., 1972. *J. Chem. Phys.*, **56**, 958.
Herbig, G. H., 1956. *Publ. astr. Soc. Pacific*, **68**, 204.
Hinkle, K. H., 1978. *Astrophys. J.*, **220**, 210.
Hinze, J., Lie, G. C. & Liu, B., 1975. *Astrophys. J.*, **196**, 621.
Hoffman, H. & Trefftz, E., 1980. *Astr. Astrophys.*, **82**, 256.
Huber, K. P. & Herzberg, G., 1979. *Constants of Diatomic Molecules*, van Nostrand Reinhold, New York.
Hudson, R. D., 1971. *Rev. Geophys. Space Phys.*, **9**, 305.
Hudson, R. D. & Carter, V. L., 1967a. *J. Opt. Soc. America*, **57**, 651.
Hudson, R. D. & Carter, V. L., 1967b. *Astrophys. J.*, **149**, 229.
Inn, E. C. Y., Watanabe, K. & Zelikoff, M., 1953. *J. Chem. Phys.*, **21**, 1648.
JANAF, 1971. NSRDS-NBS-37, US Government Printing Office, Washington D.C.
Johnson, H. L., 1967. *Astrophys. J.*, **149**, 345.

Johnson, H. R., Bernat, A. P. & Krupp, B. M., 1980. *Astrophys. J. Suppl.*, **42**, 501.
Jura, M. & Morris, M., 1981. *Astrophys. J.*, **251**, 181.
Kelly, H. P., 1972. *Phys. Rev. A.*, **6**, 1048.
Knapp, G. R., Phillips, T. G. & Huggins, P. J., 1980. *Astrophys. J.*, **242**, L25.
Lagervist, A. & Renhorn, I., 1974. *J. Molec. Spectrosc.*, **49**, 157.
Lambert, D. L. & Vanden Bout, P. A., 1978. *Astrophys. J.*, **211**, 854.
Lee, T. A., 1970. *Astrophys. J.*, **162**, 217.
Lee, L. C., 1980. *J. Chem. Phys.*, **72**, 4334.
Liszt, H. S. & Smith, W. H., 1972. *J. Quant. Spectrosc. Radiat. Transfer*, **12**, 947.
Lovas, F. J., Maki, A. G. & Olson, W. B., 1981. *J. Mol. Spectrosc.*, **87**, 449.
McCarthy, D. W., Low, F. J. & Howell, R., 1977. *Astrophys. J.*, **214**, L89.
McClintock, W., Linsky, J. L., Henry, R. C., Moos, H. W. & Gerola, H., 1975. *Astrophys. J.*, **202**, 165.
McMillan, R. S. & Tapia, S., 1978. *Astrophys. J.*, **217**, L97.
Millar, T. J., 1980. *Astrophys. Space Sci.*, **72**, 509.
Moran, J. M., Ball, J. A., Predmore, C. R., Lane, A. P., Huguenin, G. R., Reid, M. J. & Hansen, S. S., 1979. *Astrophys. J.*, **231**, L67.
Okabe, H., 1978. *Photochemistry of Small Molecules*, Wiley, New York.
Pacansky, J. & Hermann, K., 1978. *J. Chem. Phys.*, **69**, 963.
Prasad, S. S. & Huntress, W. T., 1980. *Astrophys. J. Suppl.*, **43**, 1.
Robbe, J. M., Schamps, J., Lefebvre-Brion, H. & Raseev, G., 1979. *J. Molec. Spectrosc.*, **74**, 375.
Rowan-Robinson, M. & Harris, S., 1982. *Astrophys. J. Suppl.*, in press.
Sanner, F., 1976. *Astrophys. J. Suppl.*, **32**, 115.
Saxon, R. P., Kirby, K. & Liu, B., 1980. *J. Chem. Phys.*, **73**, 1873.
Scalo, J. M. & Slavsky, D. B., 1980. *Astrophys. J.*, **239**, L73.
Seaton, M. J., 1951. *Mon. Not. R. astr. Soc.*, **111**, 368.
Shanker, R., Linton, C. & Verma, R. D., 1976. *J. Mol. Spectrosc.*, **60**, 197.
Solomon, P. M. & Klemperer, W., 1972. *Astrophys. J.*, **178**, 389.
Spencer, J. H., Winnberg, A., Olnon, F. M., Schwartz, R. R., Mathews, H. E. & Downes, D., 1981. *Astr. J.*, **86**, 392.
Stencel, R. E. & Mullan, D. J., 1980. *Astrophys. J.*, **238**, 221.
Stickland, D. J. & Sanner, F., 1981. *Mon. Not. R. astr. Soc.*, **197**, 791.
Sutton, E. C., Storey, J. W. V., Betz, A. L. & Townes, C. H., 1977. *Astrophys. J.*, **217**, L97.
Tabak, R. G., Hirth, J. P., Meyrick, G. & Roark, T. P., 1975. *Astrophys. J.*, **196**, 457.
Tan, K. H., Brion, C. E., van der Leeuw, P. E. & van der Wiel, M. J., 1978. *Chem. Phys.*, **29**, 299.
Thompson, G. I., Nandy, K., Jamar, C., Monfils, A., Houziaux, L., Carnochan, D. J. & Wilson, R., 1978. *Catalogue of Stellar UV Fluxes*, UK Science Research Council.
Tielens, A. G. G. M., 1982. *PhD thesis*, Leiden University.
Turner, J. L. & Dalgarno, A., 1977. *Astrophys. J.*, **213**, 386.
Welter, G. L. & Worden, S. P., 1980. *Astrophys. J.*, **242**, 673.
Willson, L. A. & Hill, S. J., 1979. *Astrophys. J.*, **228**, 854.
Wishart, A. W., 1979. *Mon. Not. R. astr. Soc.*, **187**, 59P.
Zuckerman, B., 1980. *A. Rev. Astr. Astrophys.*, **18**, 263.